

Robot Perception of Environment Impedance

Ryo Kikuuwe and Tsuneo Yoshikawa

Abstract—This paper proposes a novel identification technique of constraint condition that the environment imposes on the robot’s end-effector, based on position and force sensing during arbitrary manipulation. In the proposed method, the impedance that constrains the motion of the end-effector is estimated on-line; the uncertainties of the estimates are evaluated; and discontinuous changes of the impedance are detected. This method can be installed to robots as human-like perception of impedance, and can be used for monitoring human demonstration. Results of preliminary experiments are presented.

Keywords— perception of impedance, environment property estimation, constraint condition identification

I. INTRODUCTION

In executing complex manipulation tasks in uncertain environments, humans rely heavily on their visual, tactile, and haptic sensations. Though global and geometric information is obtained through vision, information on constraint that is imposed on motion of the hand or fingertip is inferred mainly through tactile and haptic sensations. For future intelligent and autonomous robots that could be used in human-centered and uncertain environments, the same kind of perceptual capability is required.

Robot’s perceptivity of constraint condition can be composed of position (motion) and force sensations. Identification of constraint condition has a close connection with that of environment, because a global model of environment can be obtained by investigating constraint conditions at multiple points. Various researches have been done for identification problems of constraint condition and environment properties by monitoring position and/or force data. Active probing operation to identify geometric relation between the grasped (manipulated) object and the environment is studied by several researchers [1], [2]. Okamura et al. studied on semi-autonomous exploration of remote environment surfaces [3]. Emura and Tachi [4] and MacLean [5] estimated dynamic properties of deformable objects by specialized control methods. Those integrated methods of sensing and control, namely ‘active’ sensing methods, enable efficient data collection and precise and accurate estimation even under the existence of noises and uncertainties. However, selection of control modes and concomitance with

manual control command from human operator could arouse other problems.

Sensing/analyzing techniques independent from control strategy, namely ‘passive’ sensing methods, are less efficient but can provide easier solution for broader range of applications. The literature includes hidden Markov models [6], fuzzy logic and neural networks [7], and thresholding and Boolean operations [8]. Those passive sensing methods are applicable also for interpreting human-performed tasks and for analyzing human manipulation skills [9]. Dupont et al. [10] gave a solution framework for environment property estimation by monitoring position and force during a human’s manipulation. All of the above assume non-deformable and geometrically simple environments.

In this paper, we propose a novel identification technique of constraint condition based on position and force sensing during arbitrary manipulation. We deal with general deformable environment, and focus on the mechanical impedance that constrains the motion of the robot’s end-effector. In the proposed algorithm, the impedance parameters are estimated on-line. Since the observed signals are generally not sufficiently frequency-rich, the uncertainties of the estimates are evaluated to distinguish significant information. Moreover, detection of discontinuous changes of the impedance is preformed. Estimated impedance parameters can be used to identify local dynamic properties of the environment and temporary constraint condition between the robot and the environment. The detected discontinuities can be interpreted as boundaries between environment components, and as changes of constraint condition. In the rest of this paper, section II presents the algorithm of impedance perception. In section III its validity was tested by experiments. Section IV is for conclusion and for discussing potential applications.

II. ALGORITHM OF IMPEDANCE PERCEPTION

A. Model of Constraint Condition

An environment is composed of several components whose dynamic characteristics are different from each other. Generally their dynamic characteristics are not linear, but we assume that the force-motion relation can be locally approximated by a linear dynamic equation in a minute region.

Let $\mathbf{p}(t) \in \mathcal{R}^3$ be the position of the robot’s end-effector, and $\mathbf{f}(t) \in \mathcal{R}^3$ be the force applied from the

Ryo Kikuuwe and Tsuneo Yoshikawa are with the Department of Mechanical Engineering, Kyoto University, Kyoto, Japan. E-mail: {t60y0129@ip.media, yoshi@mech}.kyoto-u.ac.jp.

end-effector (strictly, the force sensor) to the environment. From the assumption, $\mathbf{p}(t)$ and $\mathbf{f}(t)$ have a relation described below;

$$\mathbf{f}(t) = \mathbf{c} + \mathbf{K}\mathbf{p}(t) + \mathbf{B}\dot{\mathbf{p}}(t) + \mathbf{M}\ddot{\mathbf{p}}(t), \quad (1)$$

where \mathbf{K}, \mathbf{B} and $\mathbf{M} \in \mathcal{R}^{3 \times 3}$ are the stiffness, viscosity and inertia matrices respectively, which are determined by dynamic properties of the end-effector and the environment, and contact configuration between them. $\mathbf{c} \in \mathcal{R}^3$ is a constant vector which corresponds to the equilibrium point of the stiffness, bias of force resulting from gravitation, and etc.

The dynamic equation (1) cannot be applied for constraint conditions where the position is fixed but the force varies, i.e. a contact between a rigid end-effector and a rigid surface. Therefore, we suppose the end-effector is virtually visco-elastic, and that its virtual position is obtained by adding a simulated displacement to the real position. The force $\mathbf{f}(t)$ is observed by the force sensor. Then, the displacement of the virtual soft effector, $\Delta\mathbf{p}_v(t)$, is simulated by solving the following dynamic equation;

$$\mathbf{f}(t) = K_v \Delta\mathbf{p}_v(t) + B_v \Delta\dot{\mathbf{p}}_v(t) \quad (2)$$

where K_v and B_v are design parameters which represent the stiffness and viscosity coefficients of the virtual soft effector. The position of the virtual soft effector is determined as follows;

$$\mathbf{p}(t) = \mathbf{p}_r(t) + \Delta\mathbf{p}_v(t), \quad (3)$$

where $\mathbf{p}_r(t)$ denotes the real position observed by the position sensors. Substituting $\mathbf{p}(t)$ in (1) with the virtual position $\mathbf{p}(t)$ from (3), even a rigid contact state can be modeled using (1).

B. Discrete Time Approximation

Taking Laplace transforms of both sides of (1) yields

$$\mathcal{L}[\mathbf{f}(t) - \mathbf{c}] = (\mathbf{K} + s\mathbf{B} + s^2\mathbf{M}) \mathcal{L}[\mathbf{p}(t)], \quad (4)$$

where \mathcal{L} denotes a Laplace transform. Moreover, by using bilinear transformation, $s := \frac{2}{T} \frac{1-z^{-1}}{1+z^{-1}}$ where T is the sampling time, (4)'s discrete-time approximation is written as follows;

$$\mathcal{Z}[\mathbf{f}(t) - \mathbf{c}] = \frac{\mathbf{L}_1 + \mathbf{L}_2 z^{-1} + \mathbf{L}_3 z^{-2}}{(1+z^{-1})^2} \mathcal{Z}[\mathbf{p}(t)], \quad (5)$$

where \mathcal{Z} denotes a Z -transform and

$$\begin{aligned} [\mathbf{L}_1 \quad \mathbf{L}_2 \quad \mathbf{L}_3]^T &\triangleq (\mathbf{T}_1 \otimes \mathbf{I}_3) [\mathbf{K} \quad \mathbf{B} \quad \mathbf{M}]^T \quad (6) \\ \mathbf{T}_1 &\triangleq \begin{bmatrix} 1 & 2/T & 4/T^2 \\ 2 & 0 & -8/T^2 \\ 1 & -2/T & 4/T^2 \end{bmatrix}. \quad (7) \end{aligned}$$

$\mathbf{X} \otimes \mathbf{Y}$ denotes the Kronecker product of $\mathbf{X} (\in \mathcal{R}^{m \times n})$ and $\mathbf{Y} (\in \mathcal{R}^{p \times q})$, which is defined by

$$\mathbf{X} \otimes \mathbf{Y} = \begin{bmatrix} x_{11}\mathbf{Y} & \cdots & x_{1n}\mathbf{Y} \\ \vdots & \ddots & \vdots \\ x_{m1}\mathbf{Y} & \cdots & x_{mn}\mathbf{Y} \end{bmatrix} \in \mathcal{R}^{mp \times nq}.$$

Thus a discrete-time approximation of (1) is obtained as follows;

$$\phi_k = \Theta^T \psi_k \quad (8)$$

$$\phi_k \triangleq \mathbf{f}_k + 2\mathbf{f}_{k-1} + \mathbf{f}_{k-2} \in \mathcal{R}^3 \quad (9)$$

$$\psi_k \triangleq [1 \quad \mathbf{p}_k^T \quad \mathbf{p}_{k-1}^T \quad \mathbf{p}_{k-2}^T]^T \in \mathcal{R}^{10} \quad (10)$$

$$\Theta \triangleq \mathbf{T}\Theta_{\mathbf{I}} \in \mathcal{R}^{10 \times 3} \quad (11)$$

$$\mathbf{T} \triangleq \left[\begin{array}{c|c} 4 & 0 \\ \hline 0 & \mathbf{T}_1 \otimes \mathbf{I}_3 \end{array} \right] \in \mathcal{R}^{10 \times 10} \quad (12)$$

$$\Theta_{\mathbf{I}} \triangleq [\mathbf{c} \quad \mathbf{K} \quad \mathbf{B} \quad \mathbf{M}]^T \in \mathcal{R}^{10 \times 3}. \quad (13)$$

A variables with subscript k denotes its value at time instant kT .

C. Weighted Least Squares Estimation

At time instant kT , a weighted sum-of-products matrix of residual errors from the model (8) is obtained as follows;

$$\begin{aligned} \mathbf{J}_k(\Theta) &\triangleq \sum_{i=i_0}^k w_{k,i} (\phi_i - \Theta^T \psi_i) (\phi_i - \Theta^T \psi_i)^T \\ &= \Theta^T \mathbf{R}_k \Theta - \mathbf{Q}_k^T \Theta - \Theta^T \mathbf{Q}_k + \mathbf{F}_k \quad (14) \end{aligned}$$

where $\{w_{k,i}\}_{i_0 \leq i \leq k}$ denotes the weighting sequence at time instant kT , i_0 is the time instant at which the calculation starts, $\mathbf{R}_k \triangleq \sum_{i=i_0}^k w_{k,i} \psi_i \psi_i^T$, $\mathbf{Q}_k \triangleq \sum_{i=i_0}^k w_{k,i} \psi_i \phi_i^T$, and $\mathbf{F}_k \triangleq \sum_{i=i_0}^k w_{k,i} \phi_i \phi_i^T$. Design of the weighting sequence is discussed in II-E. When \mathbf{R}_k^{-1} exists, (14) is transformed as follows;

$$\mathbf{J}_k(\Theta) = (\Theta - \hat{\Theta}_k)^T \mathbf{R}_k (\Theta - \hat{\Theta}_k) + \mathbf{S}_k \quad (15)$$

$$\hat{\Theta}_k \triangleq \mathbf{R}_k^{-1} \mathbf{Q}_k \quad (16)$$

$$\mathbf{S}_k \triangleq \mathbf{F}_k - \mathbf{Q}_k^T \mathbf{R}_k^{-1} \mathbf{Q}_k \quad (17)$$

Since \mathbf{R}_k is positive definite, $\mathbf{J}_k(\Theta) \succeq \mathbf{J}_k(\hat{\Theta}_k) = \mathbf{S}_k$ is satisfied with any Θ ($\mathbf{X} \succeq \mathbf{Y}$ means that $\mathbf{X} - \mathbf{Y}$ is positive semi-definite). Therefore, we adopt $\hat{\Theta}_k$ as the estimate of Θ at time instant kT . Since the relation between Θ and $\Theta_{\mathbf{I}}$ is described by (11), the estimate of $\Theta_{\mathbf{I}}$ is given by $\hat{\Theta}_{\mathbf{I},k} = [\hat{\mathbf{c}}_k \quad \hat{\mathbf{K}}_k \quad \hat{\mathbf{B}}_k \quad \hat{\mathbf{M}}_k]^T = \mathbf{T}^{-1} \hat{\Theta}_k$.

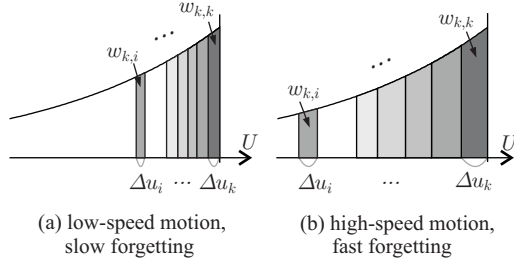


Fig. 1. Scale of forgetting and weighting sequence

D. Estimation of Uncertainty

Recall that $\mathbf{J}_k(\Theta) \succeq \mathbf{S}_k$. Thus we assume that $D_k(\Theta)$, a difference measure from $\hat{\Theta}_k$ to a given Θ , can be given by

$$\begin{aligned} D_k(\Theta) &= \text{tr} \left[\mathbf{S}_k^{-\frac{1}{2}} (\mathbf{J}_k(\Theta) - \mathbf{S}_k) \mathbf{S}_k^{-\frac{1}{2}} \right] \\ &= \text{cs} \left[\Theta - \hat{\Theta}_k \right]^T \hat{\Pi}_k^{-1} \text{cs} \left[\Theta - \hat{\Theta}_k \right] \quad (18) \end{aligned}$$

$$\hat{\Pi}_k \triangleq \mathbf{S}_k \otimes \mathbf{R}_k^{-1}. \quad (19)$$

$\text{cs}[\mathbf{X}]$ denotes the column string of \mathbf{X} ($\in \mathcal{R}^{m \times n}$), which is defined by

$$\text{cs}[\mathbf{X}] = [\mathbf{x}_1^T \ \cdots \ \mathbf{x}_n^T]^T \in \mathcal{R}^{mn},$$

where \mathbf{x}_i ($\in \mathcal{R}^m$) represents i -th column of \mathbf{X} . With a design parameter $A (> 0)$, the set of Θ which satisfy $D_k(\Theta) \leq A$ is denoted as a hyper-ellipsoid;

$$\text{cs} \left[\Theta - \hat{\Theta}_k \right]^T \hat{\Pi}_k^{-1} \text{cs} \left[\Theta - \hat{\Theta}_k \right] \leq A. \quad (20)$$

Since (11), (20) is transformed as follows;

$$\text{cs} \left[\Theta_{\text{I}} - \hat{\Theta}_{\text{I},k} \right]^T \hat{\Pi}_{\text{I},k}^{-1} \text{cs} \left[\Theta_{\text{I}} - \hat{\Theta}_{\text{I},k} \right] \leq A \quad (21)$$

$$\hat{\Pi}_{\text{I},k} = \mathbf{S}_k \otimes \left(\mathbf{T} \mathbf{R}_k^{-1} \mathbf{T}^T \right) \quad (22)$$

Thus the uncertainty of $\hat{\Theta}_k$ is evaluated by $\hat{\Pi}_k$, and that of $\hat{\Theta}_{\text{I},k}$ by $\hat{\Pi}_{\text{I},k}$.

E. Forgetting Factor Depending on Speed of Movement

Since real environments have non-linear features, the coefficient matrices in (1) can gradually vary according to position. Therefore, the weighting sequence $\{w_{k,i}\}_{i_0 \leq i \leq k}$ has to be chosen so that old data are discounted. Recursive least squares method with forgetting factor is commonly used in this kind of situations. In this conventional method, observed data are ‘forgotten’ according to elapsed time. Thus, when this method with constant forgetting speed is applied here,

low-speed motion sometimes results in too narrow distribution of sampled points in space domain. In order to avoid this problem, we employ forgetting factor that varies according to the speed of movement.

We assume that forgetting occurs exponentially, as shown in Fig.1. The update rule of weights $w_{k,i}$ is described as follows;

$$w_{k,i} = \begin{cases} 1 - r_k & , \text{ if } i = k \\ r_k w_{k-1,i} & , \text{ if } i < k \end{cases} \quad (23)$$

$$r_k = 2^{-\Delta u_k}, \quad (24)$$

where $\Delta u_k > 0$ can be referred to as distance between instants kT and $(k-1)T$ evaluated on *scale of forgetting* (the U axis in Fig.1). Using this rule, $W_k \triangleq \sum_{i=i_0}^k w_{k,i}$ increases monotonously and converges to 1 as $k \rightarrow \infty$. Δu_k is defined as follows so that low-speed motion makes slow forgetting;

$$\Delta u_k = \min \left(\frac{T}{T_H}, \frac{\|\mathbf{p}_k - \mathbf{p}_{k-1}\|}{X_H} \right), \quad (25)$$

where T_H and X_H are design parameters, which can be referred to as half-lives in time and space domains respectively. The physical meanings of (23),(24) and (25) are that low-speed motion ($\|\dot{\mathbf{p}}_k\| \leq X_H/T_H$) makes slow forgetting and a small weight on current observed values, and that high-speed motion ($\|\dot{\mathbf{p}}_k\| > X_H/T_H$) brings forgetting at a constant rate. Using $w_{k,i}$ defined above, \mathbf{R}_k , \mathbf{Q}_k and \mathbf{F}_k are recursively updated as follows;

$$\mathbf{R}_k = r_k \mathbf{R}_{k-1} + (1 - r_k) \psi_k \psi_k^T \quad (26)$$

$$\mathbf{Q}_k = r_k \mathbf{Q}_{k-1} + (1 - r_k) \psi_k \phi_k^T \quad (27)$$

$$\mathbf{F}_k = r_k \mathbf{F}_{k-1} + (1 - r_k) \phi_k \phi_k^T \quad (28)$$

F. Discontinuity Detection

Discontinuous changes of constraint condition is detected by checking whether the current observed data match a past estimate. At time instant k , we choose a referential past instant $\kappa(k)$ as follows;

$$\kappa(k) = \kappa \quad \text{s.t.} \quad U = \sum_{i=\kappa+1}^k \Delta u_i \quad (29)$$

where U is a design parameter.

The estimate of ϕ_k based on the estimated model at $\kappa(k)$ is described as $\hat{\phi}_{k|\kappa(k)} \triangleq \hat{\Theta}_{\kappa(k)}^T \psi_k$. From (8), the difference between observed and estimated vectors $\tilde{\phi}_{k|\kappa(k)} \triangleq \phi_k - \hat{\phi}_{k|\kappa(k)} = (\Theta - \hat{\Theta}_{\kappa(k)})^T \psi_k$ is described as follows;

$$\tilde{\phi}_{k|\kappa(k)} = (\mathbf{I}_3 \otimes \psi_k^T) \text{cs} \left[\Theta - \hat{\Theta}_{\kappa(k)} \right] \quad (30)$$

If and only if $D_{\kappa(k)}(\Theta) \leq A$ holds, we have

$$\text{cs} \left[\Theta - \hat{\Theta}_{\kappa(k)} \right] \text{cs} \left[\Theta - \hat{\Theta}_{\kappa(k)} \right]^T \preceq A \hat{\Pi}_{\kappa(k)} \quad (31)$$

since (20). Considering (30), we have

$$\begin{aligned} \tilde{\Phi}_{k|\kappa(k)} \tilde{\Phi}_{k|\kappa(k)}^T &\preceq A (\mathbf{I}_3 \otimes \psi_k^T) \Pi_{\kappa(k)} (\mathbf{I}_3 \otimes \psi_k) \\ &= A (\psi_k^T \mathbf{R}_{\kappa(k)}^{-1} \psi_k) \mathbf{S}_{\kappa(k)}, \end{aligned} \quad (32)$$

and the above is equivalent to

$$e_{k|\kappa(k)} \triangleq \frac{1}{A} \frac{\tilde{\Phi}_{k|\kappa(k)}^T \mathbf{S}_{\kappa(k)}^{-1} \tilde{\Phi}_{k|\kappa(k)}}{\psi_k^T \mathbf{R}_{\kappa(k)}^{-1} \psi_k} \leq 1. \quad (33)$$

We assume that when $e_{k|\kappa(k)} > 1$ hold at all instants $k = \kappa(k_c) + 1, \dots, k_c$, instants $\kappa(k_c)$ and k_c are under different constraint conditions. In other words, discontinuous change at instant $\kappa(k_c)$ is detected at instant k_c .

An estimate that is based on a time range including a discontinuity makes no sense. Therefore, when the discontinuities are detected, all the elements of \mathbf{R}_k , \mathbf{Q}_k and \mathbf{F}_k are set to be 0.

III. EXPERIMENT

In order to test the validity of the algorithm described above, preliminary experiments were conducted. The overview of the setup is as shown in Fig.2. It is composed of a three-joint miniature robot arm ‘‘Mini-Robot’’ (Daikin Industries Ltd.), a 6-axis force-torque sensor (‘‘NANO Sensor’’, BL Autotec, LTD.), and an acrylic ball (a table tennis ball of diameter 38[mm]), which is used as the end-effector. The position of the end-effector is measured by optical encoders (500P/R type) attached to joints through reduction gears of ratio 1:8. In the experiments, the joint actuators are not driven, but the robot arm is moved directly by the experimenter with his hand as shown in Fig.2.

Two experiments were conducted. Experiment I is mainly to test the ability to detect changes in stiffness, where a weighing machine is used as shown in Fig.3(a)(b). When an applied force exceeds about 4.9[N], its moving part gets in contact with its frame and it behaves as a rigid body as shown by C in Fig.3(b)). The procedure is as follows;

1. (step A) Move the effector in $-z$ direction until it gains contact with the weighing machine.
2. (step B) Push the effector further down in $-z$ direction until the moving part of the weighing machine gets in touch with the frame.
3. (step C) Keep the rigid contact between the moving part and the frame of the weighing machine.

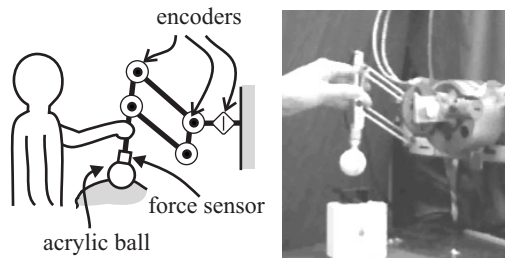


Fig. 2. Experimental Setup

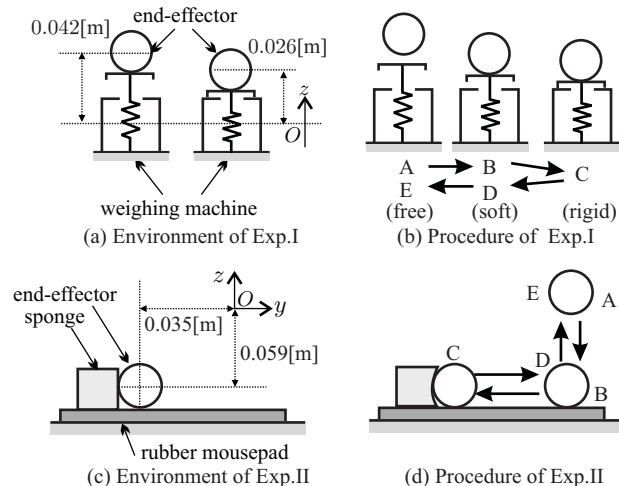


Fig. 3. Procedures of Experiments

4. (step D) Reducing the pushing force, make the moving part apart from the frame and move the effector in $+z$ direction.
5. (step E) Make the effector apart from the weighing machine, and move it further up in $+z$ direction in free space.

Experiment II is mainly to test the ability to distinct constrained directions, where a smooth rubber board (a mousepad) and a piece of sponge are used as shown in Fig.3(c)(d). The procedure is as follows;

1. (step A) Move the effector in $-z$ direction until it gets in touch with the mousepad.
2. (step B) Slide the effector on the mousepad in $-y$ direction until it gets in touch with the sponge.
3. (step C) Keeping the effector in touch with the sponge and the mousepad, push the effector into the sponge for several times.
4. (step D) Make the effector apart from the sponge, and slide it on the mousepad in $+y$ direction.
5. (step E) Make the effector apart from the mousepad, and move it in $+z$ direction in free space.

Steps A, \dots , E above corresponds to A, \dots , E in Fig.3. Values of parameters used in these experiments are

TABLE I
PARAMETERS FOR EXPERIMENT

symbol	T	K_v	B_v	X_H	T_H	U	A
value	0.002	700	10	0.001	0.1	1.0	0.5
unit	s	N/m	Ns/m	m	s	-	-

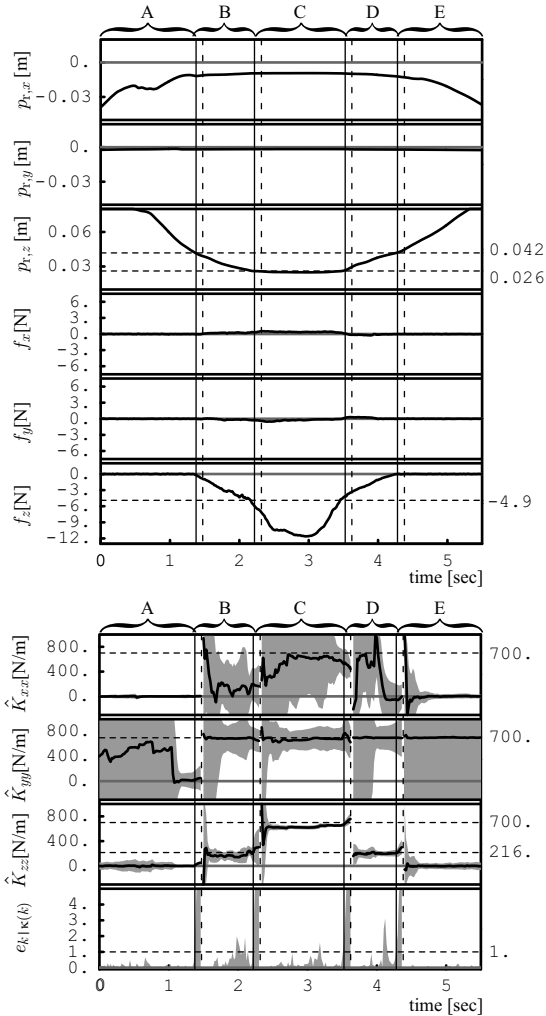


Fig. 4. Result of Experiment I

shown in Table. I. Those parameters are designed by trial and error.

A. Result

The results of Experiment I and II are shown in Fig.4 and Fig.5 respectively. $p_{r,*}$, f_* , and \hat{K}_{**} represent the elements of $\mathbf{p}_{r,k}$, \mathbf{f}_k , and $\hat{\mathbf{K}}_k$ respectively. $e_{k|\kappa(k)}$ is a difference measure between observed and estimated vectors defined by (33). Due to space limitation, only a portion out of 30 total elements of $\hat{\Theta}_{I,k}$ are shown. In the graphs of \hat{K}_{**} , black solid curves represent their values and the width of the gray bands rep-

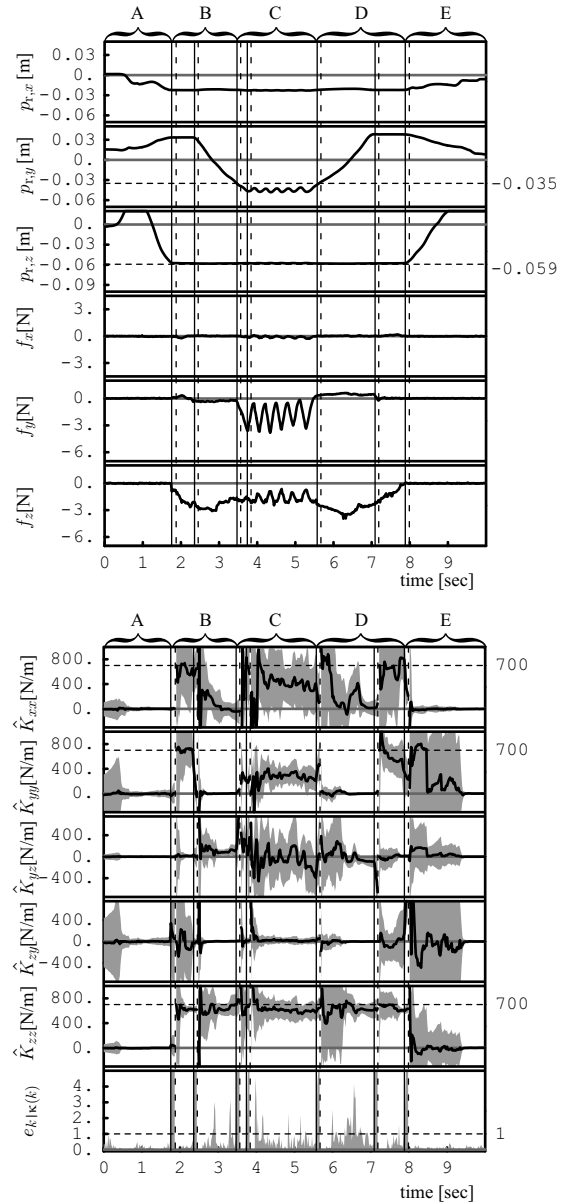


Fig. 5. Result of Experiment II

resent their uncertainties, that are their correspondent diagonal elements of $A\hat{\Pi}_{I,k}$. Note that large width of the bands means lower significancy of the estimates. The vertical dotted lines represent k_c 's, instants at which discontinuities are detected, and the solid lines just before them represent $\kappa(k_c)$'s, instants at which discontinuities are estimated to have occurred. A, B, ... on the tops of the graphs are correspondent to those in Fig.3.

In Fig.4, it is shown that the state transitions, gain and loss of contact with the moving part and the frame of the weighing machine, are properly de-

tected. In regions A and E, the effector is not constrained and movement in z direction is large, thus \hat{K}_{zz} has a significant value around zero. In regions B and D, \hat{K}_{zz} has a significant value which is explained from the stiffness of the weighing machine; since its real stiffness is about 312[N/m], its apparent stiffness observed through the virtual soft effector is to be $312K_v/(312 + K_v) \approx 216$ [N/m]. In region C, \hat{K}_{zz} has significant value near K_v because of a rigid contact situation between the effector and the environment. In y direction, the variability of position data is very small. Therefore, the virtual soft effector causes a large value of \hat{K}_{yy} near K_v , but the significance of this estimate is shown to be very low. In situations of static friction, stiffness coefficients in the tangential directions of the surface tend to be large; this is apparent in \hat{K}_{yy} in regions B to D.

In Fig.5, on the other hand, it is shown that gain/loss of contact with the mousepad and the sponge are properly detected, but overdetections are found at 2.356, 3.740 and 7.090[sec]. Detections at 2.356 and 7.090[sec] are caused by transitions between static and dynamic frictional states. Detection at 3.740[sec] is presumably caused by nonlinear feature of the sponge. In regions B to D, \hat{K}_{zz} has significant value near K_v , since there exists an almost rigid constraint in z direction. In region C, \hat{K}_{yy} has significant value which is smaller than \hat{K}_v , since the end-effector is in contact with a soft object. Due to the small variability of position data in x direction, significance of the estimate of \hat{K}_{xx} is low.

IV. CONCLUSION

This paper describes an algorithm of robot perception of impedance, by which the impedance parameters are estimated on-line from force and position data during arbitrary manipulation, and their discontinuities are detected. Preliminary experiments were conducted, and the results indicate the validity of the algorithm.

Human is capable of perceiving impedance by integrating position and force sensations of his/her limbs. For future autonomous and intelligent robots, the proposed technique can play a similar role. As human unconsciously exploits that perceptivity in everyday life, the proposed technique will help robot to obtain deeper understanding on the environment, to generate appropriate actions according to circumstances, and to naturally communicate with humans.

Telemanipulation could be included in the range of application. In teleoperation systems, information is transferred to the operator visually and, in limited cases, haptically. Visually recognizing the constraint state and the environment's local and dynamic prop-

erties is not easy, and haptic information can be affected by the performance of the master manipulator. Remote-manipulator's perception of impedance could enable adequate selective information display to the operator, and could reduce the operator's involvement in task execution.

For fully manually controlled robots, this perception could help understandings on the performed tasks as well. Detected discontinuities can be used for segmenting the performed action into several meaningful elementary actions. This enables understandings on the elementary actions in correspondence with the constraint conditions. To observe human demonstrations, bilateral master-slave system or a hand tool instrumented with position and force sensor can be used. Koeppel et al. 's "TeachDevice"[11] could be an example for the latter type of observation tool.

REFERENCES

- [1] T. Yoshikawa, Y. Yu, and M. Koike, "Estimation of Contact Position between Object and Environment Based on Probing of Robot Manipulator," in *Proc. of the IEEE/RSJ Int. Conf. on Intelligent Robots and Systems*, 1996, vol. 2, pp. 769-776.
- [2] T. Mouri, T. Yamada, N. Mimura, and Y. Funahashi, "Identification of Contact Conditions from Contaminated Data of Contact Moment," in *Proc. of the 1999 IEEE Int. Conf. on Robotics and Automation*, 1999, pp. 585-591.
- [3] A. M. Okamura, M. A. Costa, M. L. Turner, and C. Richard, "Haptic Surface Exploration," in *Experimental Robotics VI*, P. Corke and J. Trevelyan, Eds., vol. 250 of *Lecture Notes in Control and Information Science*, pp. 423-432. Springer-Verlag, 2000.
- [4] S. Emura and S. Tachi, "Simultaneous Measurement of Shape and Mechanical Impedance of an Object," *Journal of the Robotics Society of Japan*, vol. 15, no. 7, pp. 997-1003, 1997, (in Japanese).
- [5] K. E. MacLean, "The 'Haptic Camera': A Technique for Characterizing and Playing Back Haptic Properties of Real Environments," in *Proc. of the ASME Dynamic Systems and Control Division*, 1996, vol. 58, pp. 459-467.
- [6] G. E. Hovland and B. J. McCarragher, "Frequency-Domain Force Measurements for Discrete Event Contact Recognition," in *Proc. of the 1996 IEEE Int. Conf. on Robotics and Automation*, 1996, pp. 1166-1171.
- [7] M. Skubic and R. A. Volz, "Identifying Single-Ended Contact Formations from Force Sensor Patterns," *IEEE Transactions on Robotics and Automation*, vol. 16, no. 5, pp. 597-602, 2000.
- [8] B. J. McCarragher and H. Asada, "Qualitative Template Matching Using Dynamic Process Models for State Transition Recognition of Robotic Assembly," *J. of Dynamic Systems, Measurement, and Control*, vol. 115, pp. 261-269, 1993.
- [9] B. J. McCarragher, "Force Sensing from Human Demonstration Using a Hybrid Dynamical Model and Qualitative Reasoning," in *Proc. of the 1994 IEEE Int. Conf. on Robotics and Automation*, 1994, pp. 557-563.
- [10] P. Dupont, T. M. Schuteis, P. A. Millman, and R. D. Howe, "Automatic Identification of Environment Haptic Properties," *Presence*, vol. 8, no. 4, pp. 394-411, 1999.
- [11] R. Koeppel, A. Breidenbach, and G. Hirzinger, "Skill Representation and Acquisition of Compliant Motions using a Teach Device," in *Proc. of the IEEE/RSJ Int. Conf. on Intelligent Robots and Systems*, 1996, pp. 897-904.